Journal of ELECTRONIC MATERIALS, Vol. 45, No. 12, 2016
DOI: 10.1007/s11664-016-4837-2

Al and Si Alloying Effect on Solder Joint Reliability in Sn-0.5Cu for Automotive Electronics

WON SIK HONG,[1,3] CHULMIN OH,[1] MI-SONG KIM,[1] YOUNG WOO LEE,[2] HUI JOONG KIM,[2] SUNG JAE HONG,[2] and JEONG TAK MOON[2]

1.—Electronic Convergence Materials and Device Research Center, Korea Electronics Technology Institute (KETI), #25, Saenari-ro, Bundang-gu, Seongnam-si, Gyeonggi-do 13509, Republic of Korea. 2.—MK Electron Co., Ltd., Yongin-si, Gyeonggi-do 17030, Republic of Korea. 3.—e-mail: wshong@keti.re.kr

To suppress the bonding strength degradation of solder joints in automotive electronics, we proposed a mid-temperature quaternary Pb-free Sn-0.5Cu solder alloy with minor Pd, Al, Si and Ge alloying elements. We manufactured powders and solder pastes of Sn-0.5Cu-(0.01,0.03)Al-0.005Si-(0.006–0.007)Ge alloys (T_m = 230°C), and vehicle electronic control units used for a flame-retardant-4 printed circuit board with an organic solderability preservative finish were assembled by a reflow soldering process. To investigate the degradation properties of solder joints used in engine compartments, thermal cycling tests were conducted from −40°C to 125°C (10 min dwell) for 1500 cycles. We also measured the shear strength of the solder joints in various components and observed the microstructural evolution of the solder joints. Based on these results, intermetallic compound (IMC) growth at the solder joints was suppressed by minor Pd, Al and Si additions to the Sn-0.5Cu alloy. After 1500 thermal cycles, IMC layers thicknesses for 100 parts per million (ppm) and 300 ppm Al alloy additions were 6.7 μm and 10 μm, compared to the as-reflowed bonding thicknesses of 6 μm and 7 μm, respectively. Furthermore, shear strength degradation rates for 100 ppm and 300 ppm Al(Si) alloy additions were at least 19.5%–26.2%. The cause of the improvement in thermal cycling reliability was analyzed using the (Al,Cu)-Sn, Si-Sn and Al-Sn phases dispersed around the Cu_6Sn_5 intermetallic at the solder matrix and bonding interfaces. From these results, we propose the possibility of a mid-temperature Sn-0.5Cu(Pd)-Al(Si)-Ge Pb-free solder for automotive engine compartment electronics.

Key words: Automotive electronics, Pb-free, solder joint, degradation, end-of-life vehicles (ELV)

INTRODUCTION

Pb-free solder has been widely used since 2006 in electronic assemblies because of restrictions on the use of hazardous substances (RoHS). However, Pb-free automotive electronics are still in the early stages due to end-of-life vehicle (ELV) banning.[1] As a result of ELV banning from 2016, automotive electronics have to use Pb-free solder; however, automotive electronics still use eutectic solder and surface finishes based on the exception to ELV banning. Thus, in this work, we present the implementation of Pb-free solder in automotive electronics. Sn-3.0Ag-0.5Cu (SAC305) solder, which is well known as a replacement alloy for eutectic solder, is already utilized in electronics.[2]

Most cabin electronics in the automotive industry are normally used in the temperature range of −40°C to 85°C.[3] Therefore, it is generally possible to use SAC305 solder alloy in vehicle cabin electronics, because of the similar operating conditions between

(Received May 4, 2016; accepted July 28, 2016; published online August 15, 2016)

home appliances and hand-held electronics. As SAC305 solder has already been verified as being reliable in solder joints, many studies featuring the possibility of its adaptation to cabin electronics are likely to be published. The normal operating temperatures of an engine compartment or engine-mounted electronics are around 110°C–120°C. The environment conditions demanded for car electronics range from −40°C to 125°C, with a temperature deviation (ΔT) that can reach 165°C.[3–9] For car electronics mounted on an engine, the degradation rate of the SAC305 solder joint shows different degradation properties. Thus, we developed a mid-temperature Pb-free solder alloy that has stable degradation properties (bonding strength, thermo-mechanical fatigue life and metallurgical stability) and a long service lifetime under high operation temperatures and thermal cycling conditions.[3–9]

Many previous studies have attempted to improve the solder joint reliability using minor additions of Pd, Bi, Sb, In, Al, Si and Ca to Sn-based solder alloys.[10–17] Even though mid-temperature Pb-free solder alloys, with a melting temperature of around 220°C, can be used to replace eutectic solder in cabin electronics, they are otherwise hard to utilize in engine compartment electronics due to the rapid degradation of solder joint strength.[8,9] In recent papers, the Al and Si addition to SAC or Sn-0.5Cu solders have been studied to improve the mechanical properties and to increase the melting temperature.[24–27] When 0.1 wt.%–0.6 wt.% Al was added to commercial Sn-0.7Cu solder, the modified solder improved the ductility.[26] Sabri et al. also report that 0.1 wt.%–0.5 wt.% Al addition increased the ductility and toughness for Sn-1Ag-0.5Cu solder alloy.[24,25] Koo et al.[24] also studied the Al(Si) addition effect to Sn-0.5Cu solder. As 0.01 wt.%–0.05 wt.% Al was added to the Sn-0.5Cu solder, the melting temperature was increased to 230°C due to induce the formation of Cu–Al IMC and suppressed the formation of eutectic β–Sn+Cu_6Sn_5 networks in the Sn-0.5Cu solder matrix.[24] Lee et al.[11] published the effect of Pd addition on the SAC solder. In the case of Pd addition to the SAC305 solder, high-*G* shock performance of the ball grid array (BGA) was discussed without the Pd SAC305 solder joint. The results revealed that Pd-addition solder joints showed more grain refinement, recrystallization, and mechanical twin deformation during the shock test due to the suppressing of the coarsening rate of the Ag3Sn IMC particles.[11] Even though previous studoesy of Ge addition effect have not been sufficient, Ge is normally used in industry for improving the solderability of bulk solder alloy. The addition range of Ge is a very small amount similar to the impurity level.

Therefore, to develop a solder alloy for automotive engine compartment electronics, we investigated the effect of minor additions of Al, Si, Pd and Ge to Sn-0.5Cu (SC) alloy (U.S. Patent No. 9,156,111 B2),[19] which has a cost advantage because of the elimination of Ag and a 10°C higher melting temperature than SAC305. The solder joint degradation of the proposed Sn-0.5Cu(Pd)-Al(Si)-Ge was observed for its microstructural evolution, and we also measured the IMC thickness and shear strength degradation of solder joints after 1500 thermal cycles under typical environmental conditions for automotive engine compartment electronics. Based on these results, we have found that the IMC growth of the Sn-0.5Cu(Pd)-Al(Si)-Ge solder joint is suppressed and shear strength degradation is decreased in conditions within the engine compartment. These results mean that the proposed solder alloy, with a small amount of Pd, Al, Si and Ge alloying, can be applicable to automotive electronics used in harsh environments.

EXPERIMENTAL

Alloy Design and Preparation

The chemical compositions and melting temperatures of the proposed Pb-free solder alloys are indicated in Table I. The major alloying elements of this solder were composed of tin and copper (Sn-0.5Cu), which are significantly cheaper than SAC305. In particular, we reused the Sn-0.5Cu(Pd) wire bonding material which contained 0.005 wt.%–0.007 wt.% Pd. Palladium was reported to improve the shock performance and suppress IMC growth at the solder joint.[10,11] In addition, to increase the high-temperature reliability of engine compartment electronics, we added 0.01 wt.% Al (alloy 1), 0.03 wt.% Al (alloy 2), and Si and Ge were, respectively, included at 0.005–0.007 and 0.006–0.008 wt.% to improve the wettability. A more detailed explanation of the role and characteristics of the alloying elements is featured in "Results and Discussion". We manufactured a bulk solder using a

Table I. Summary of alloy compositions and their respective melting temperatures

Solder alloys		Chemical composition (wt.%) Sn	Cu	Al	Pd	Ge	Melting temp. (°C)
Alloy 1	Sn-0.5Cu(Pd)-0.01Al(Si)-0.006Ge (100 ppm Al)	Bal	0.5617	0.0139	0.005–0.007	0.0061	226.40–231.04
Alloy 2	Sn-0.5Cu(Pd)-0.03Al(Si)-0.007Ge (300 ppm Al)	Bal	0.4981	0.0340	0.005–0.007	0.0075	226.78–232.29

vacuum induction melting furnace from the MK Electronics (Gyeonggido, South Korea) under a 2×10^{-2} torr vacuum condition at 700°C for 1 h. After melting the solder, induction coupled plasma (ICP, 715 Series; Agilent) analysis was conducted to confirm the chemical composition of the bulk solder (Table I). Based on the differential scanning calorimetry (DSC, DSC-60; Shimadzu) analysis results with 10°C/min heating rate, the melting temperatures (T_m, onset temperature in the DSC curves) of solder alloys 1 and 2 were 226.4°C–232.2°C (Fig. 1).

Test Components, Vehicles and Assembly

To compare the bonding strength degradation of the solder joints of alloys 1 and 2, test coupons were soldered with 430- to 450-μm-diameter solder balls, which were manufactured by MK Electronics. The PCB materials were FR-4 with a 1.2 mm thickness and a glass transition temperature (T_g) of 145°C; the pad diameter and thickness of the PCB were 400 μm and 20 μm, respectively. The surface finish of the PCB was an OSP and the flux used with the rosin was mildly activated (RMA) standard type. A total of 60 solder balls of alloys 1 and 2 were soldered with each test vehicle, which was assembled via a reflow soldering process. The soldering process was performed at a peak temperature of 260°C for 73 s after preheating for 73 s at temperatures ranging from 150°C to 200°C. Figure 2 shows the as-reflowed test vehicles soldered with balls of alloys 1 and 2.

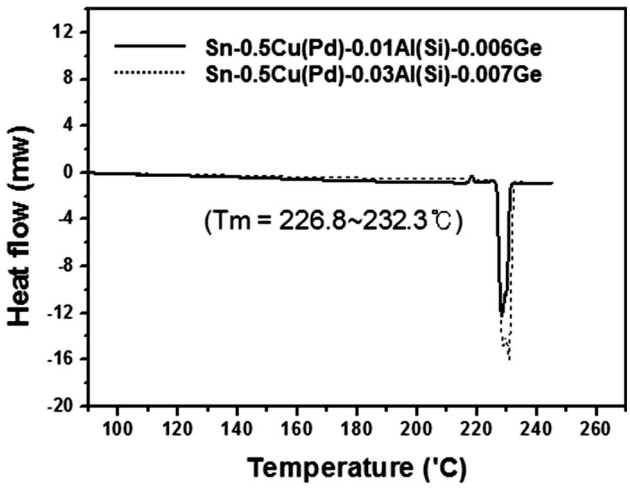

Fig. 1. Representative DSC analysis results for Sn-0.5Cu(Pd)-(0.001 and 0.03)Al(Si)-(0.006–0.008)Ge alloys

Thermal Cycling Test Conditions

The shear strength degradation behavior of alloys 1 and 2 was investigated using thermal cycling testing under typical vehicle engine compartment conditions. The thermal cycling test conditions for an engine compartment correspond to a temperature range, ramp rate, time per cycle and the number of cycles, and these conditions were set to −40°C to 125°C (board temperature: −42°C to 128°C), 33°C/min, 25 min/cycle and 1500 cycles, respectively. Figure 3a shows a temperature profile and the test equipment set-up in the chamber (Climate) for thermal cycling testing.

Shear Strength, Void Content Measurements and Microstructure Analysis of Solder Joints

The shear strength was measured by a bonding tester (Dage 4000, Nordson DAGE) for up to 1500 thermal cycles and was taken as the mean value of the strengths of ten solder balls on the same test vehicle for the as-reflowed samples with 700, 1000

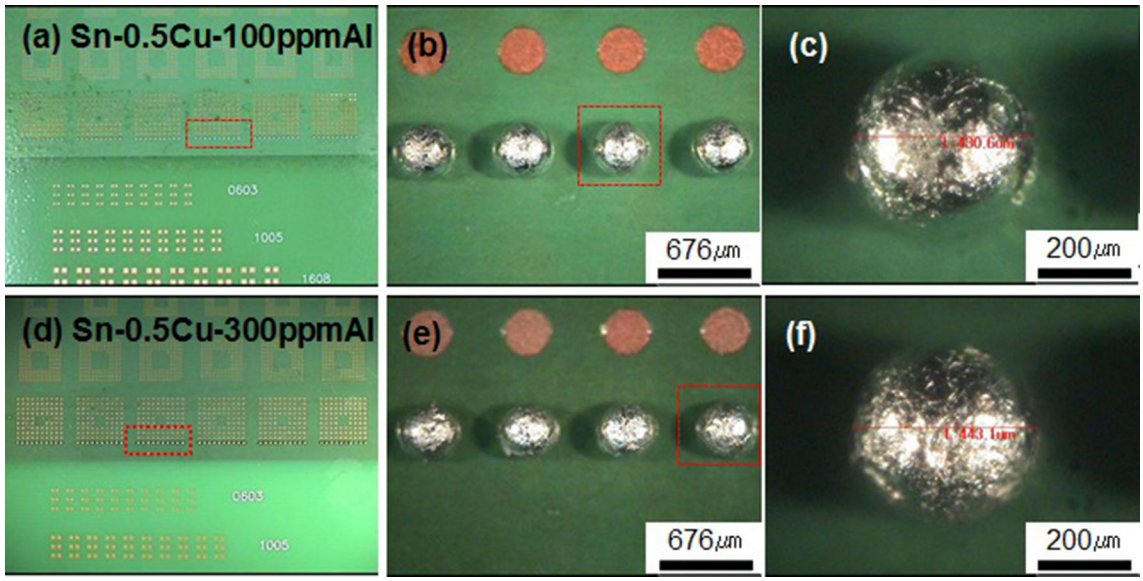

Fig. 2. Test vehicles soldered with (a–c) Sn-0.5Cu(Pd)-0.01Al(Si)-Ge and (d–f) Sn-0.5Cu(Pd)-0.03Al(Si)-Ge solder balls.

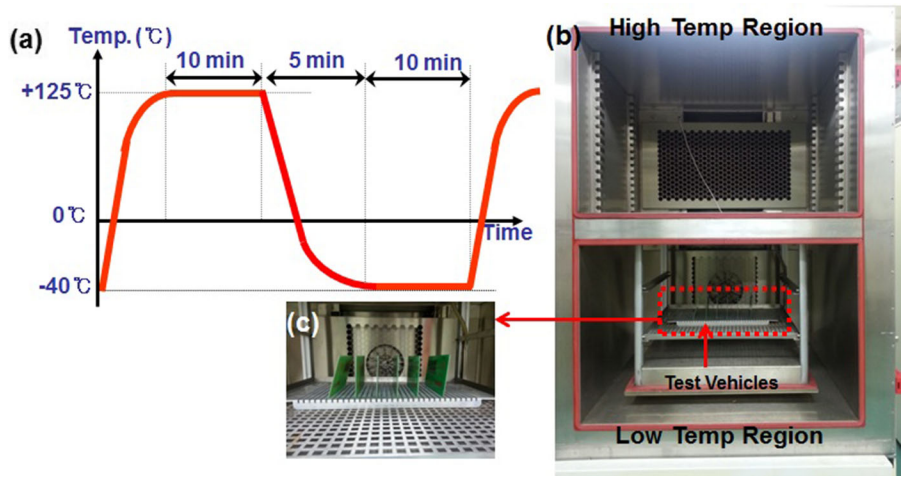

Fig. 3. (a) Temperature profile and (b, c) test equipment set-up for thermal cycling tests.

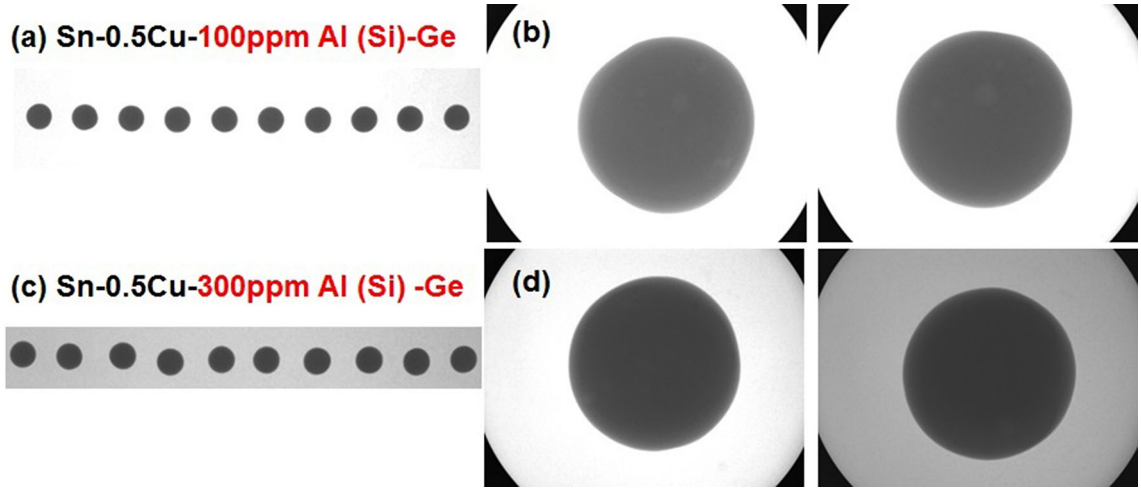

Fig. 4. X-ray non-destructive analysis images with aluminum contents of Sn-0.5Cu(Pd)-Al(Si)-Ge solder joints: (a, b) 100 ppm Al and (c, d) 300 ppm Al alloy addition.

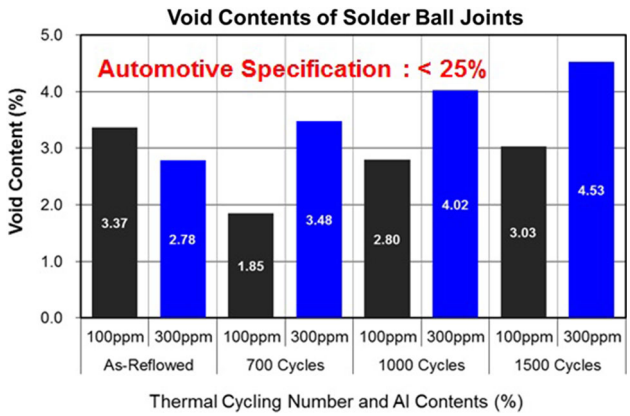

Fig. 5. Void contents comparison of 100 ppm and 300 ppm Al contained in Sn-0.5Cu(Pd)-Al(Si)-Ge solder joints.

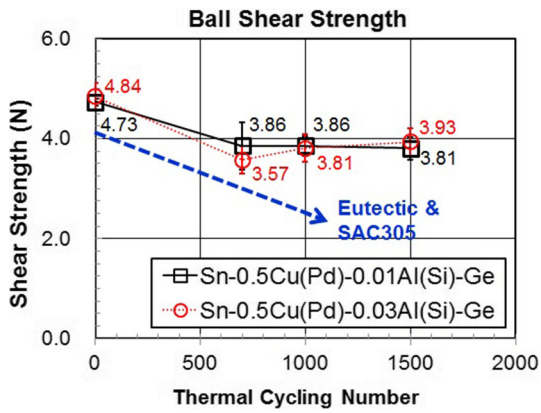

Fig. 6. Comparison of shear strength of Sn-0.5Cu(Pd)-Al(Si)-Ge solder alloy with 100 ppm and 300 ppm Al and minor Si addition under thermal cycling condition.

and 1500 cycles. The shear speed and height were 300 μm/s and 20 μm from the PCB surface, respectively.

Void contents of the solder joints with alloys 1 and 2 were measured by x-ray non-destructive analysis (Revolution model; X-TEK), as shown in Fig. 4. These were calculated as the ratio of bonding area versus the void area.

The cross-sectional microstructures of the ten solder ball joints were observed by environmental scanning electron microscopy (ESEM; ESEM-FEG XL-30, FEI), while the chemical composition of IMCs and alloy phases were analyzed using energy-dispersive x-ray spectroscopy (EDS; System SIX, NORAN). The total IMC (Cu_6Sn_5 + Cu_3Sn) thickness was calculated by using the IMC area which was divided to the width in Fig. 11.

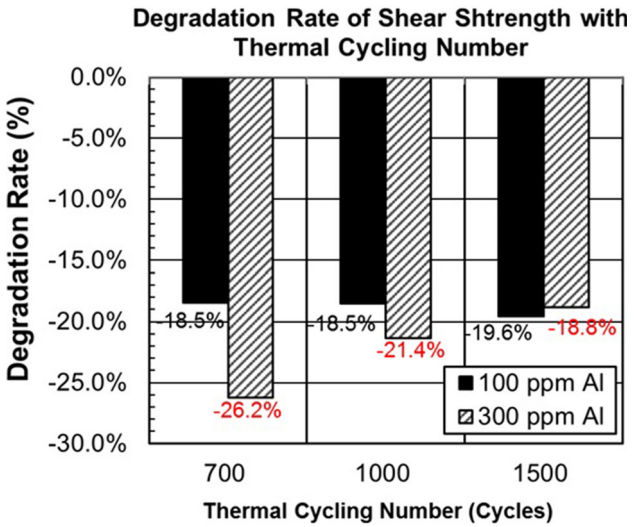

Fig. 7. Degradation rate of shear strength of solder joints with thermal cycling number.

RESULTS AND DISCUSSION

Void Content of Solder Joints

Figures 4 and 5 show the results of the void content measurements of solder joints with Al contents using x-ray non-destructive analysis. Figure 5 shows the void content with the thermal cycling number; a void rarely existed in the solder joints, as can be seen from the photographs in Fig. 4. We judged that the deviation of void contents with thermal cycling number was caused by a variation of the initial reflow in the soldering process. We also compared the void content with Al at each thermal cycling number. Based on these results, the void contents of the solder joints of the Sn-0.5Cu(Pd)-Al(Si)-Ge alloy with 0.01 wt.% and 0.03 wt.% Al (100 and 300 parts per million; ppm) were 1.8%–3.3% and 2.7%–4.5%, respectively. The void content for alloy 1 was smaller than that of alloy 2. With increasing Al content, the void content was slightly increased within the industrial acceptance level, lower than that of 20% of the bonding area. Although Al generally obstructed the solderability, in the case of minor alloying addition, Al can improve the bonding property of the solder joint due to the grain refinement of the solder materials.[16–18] The specification of void content in car electronics is normally $<25\%$, and alloys 1 and 2 satisfied this criterion with values under 5%. Based on the void content with respect to a quarter of the recommended level for an automotive company, the solderability and spreadability of alloys 1 and 2 were sufficient in the soldering process, which

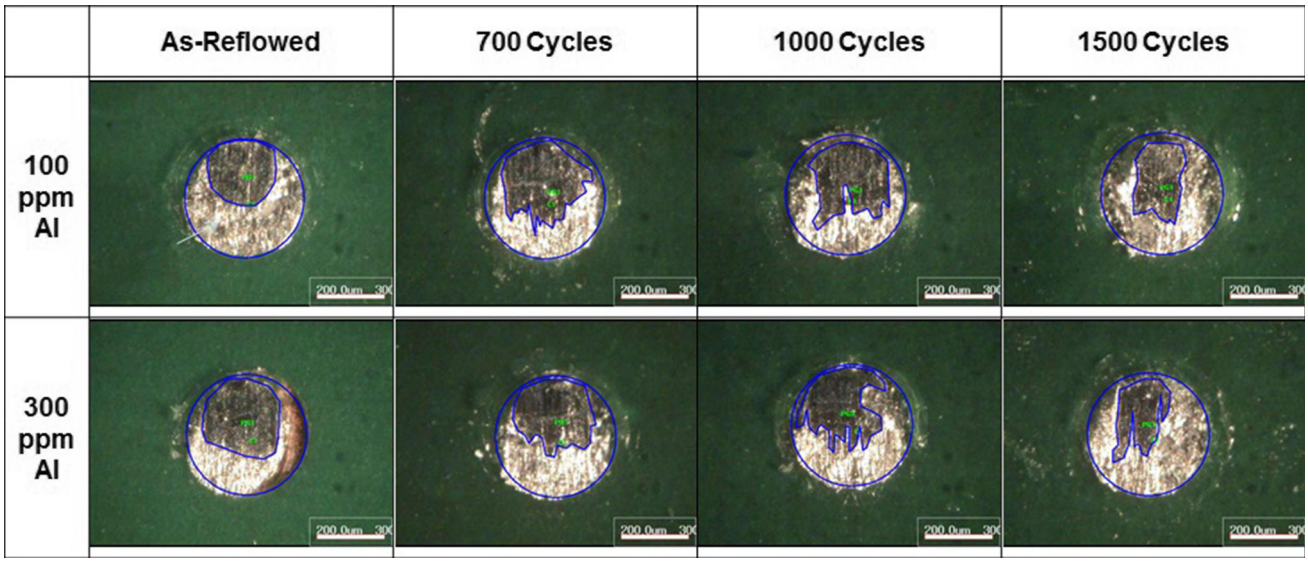

Fig. 8. Stereo micrographs of the fracture surface after shear strength tests of alloys 1 and 2 solder ball joints.

further strengthens their potential application in automotive electronics.

Shear Strength Degradation of Solder Joints with Minor Al and Si Alloying

The shear strength test results of the solder joints of alloys 1 and 2 with thermal cycling number are shown in Fig. 6. In the case of alloy 1, the initial and 700 cycles shear strength were 4.84 and 3.86 N, respectively. However, after 1000 and 1500 cycles under thermal cycling, the shear strength of alloy 1 was 3.86 N–3.81 N, so we know that there was no degradation of shear strength with the Sn-0.5Cu(Pd)-0.01Al(Si)-Ge solder. The trend shown in the alloy 2 solder is similar to alloy 1. In alloy 2, the initial shear strength was 4.84 N, which then decreased to 3.57 N after 700 cycles, but was maintained at 3.81 N after 1000 and 1500 thermal cycles. Generally, the eutectic and SAC305 solders continuously decreased the bonding strength of solder joints with thermal cycling number. Hong et al.[9] compared the shear strength degradation of chip resistors with thermal cycling number under cabin and engine compartment conditions. The shear strength of the R2012 chip resistor decreased from 63.2 to 31.6 N after 1500 thermal cycles under automotive engine compartment conditions, with a 49.3% degradation rate.[9,20,21] As revealed in Fig. 6, after 700 thermal cycles, alloys 1 and 2 never showed degradation of solder joint strength. A factor delaying the degradation is caused by the minor alloying addition of Pd, Al, Si and Ge to Sn-0.5Cu. Figure 7 shows the degradation rate of shear strength of solder joints with thermal cycling number against the initial strength. The degradation rates of TC 700, 1000 and 1500 of alloy 1 solder joints were nearly constant at −18.5%, −18.5% and −19.5%, respectively. The shear strength of alloy 2 was decreased to 700 thermal cycles, similar to alloy 1. The shear strength degradation rate of solder joints at 700, 1000 and 1500 thermal cycles versus the initial strength was decreased to −26.2%, −21.4% and −18.8%, respectively. If we compare the degradation rate of alloys 1 and 2, even though they appear similar, the degradation of a small Al-addition alloy is slightly lower than that of alloy 2. The reason for this phenomenon is due to the IMC layer thickness at the solder joint and the homogeneous microstructure.

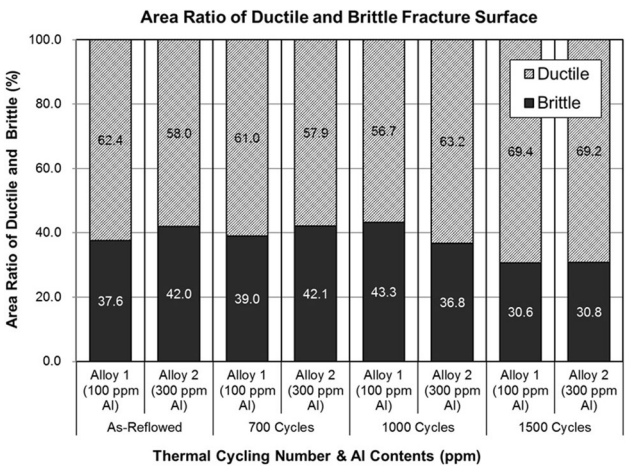

Fig. 9. Area ratio of ductile and brittle fracture surfaces of solder joints of alloys 1 and 2.

Area Ratio of Ductile and Brittle Fracture Surface with Thermal Cycling

Fracture surface analysis results after solder ball shear testing are shown in Fig. 8, while Fig. 9 shows the area ratio of ductile and brittle fracture surface based on its photographs. The Sn-Ag-Cu Pb-free solder generally indicates Cu–Sn IMC formation and decreases the bonding strength with increasing IMC thickness, and, finally, the brittle fracture of the solder joint is increased with the

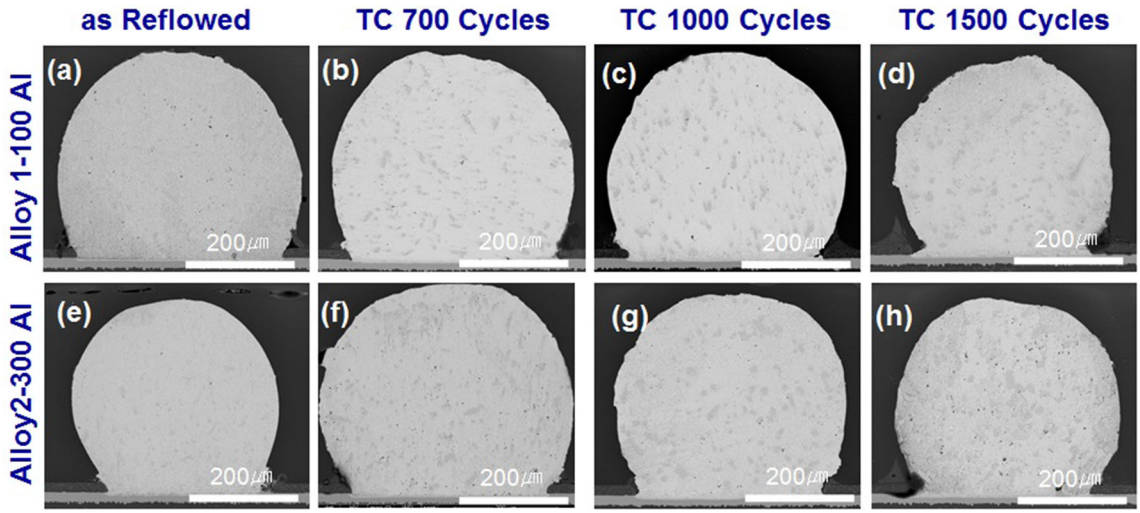

Fig. 10. Cross-sectional micrographs of (a–d) alloys 1 and (e–h) alloy 2 solder ball joints with thermal cycling number.

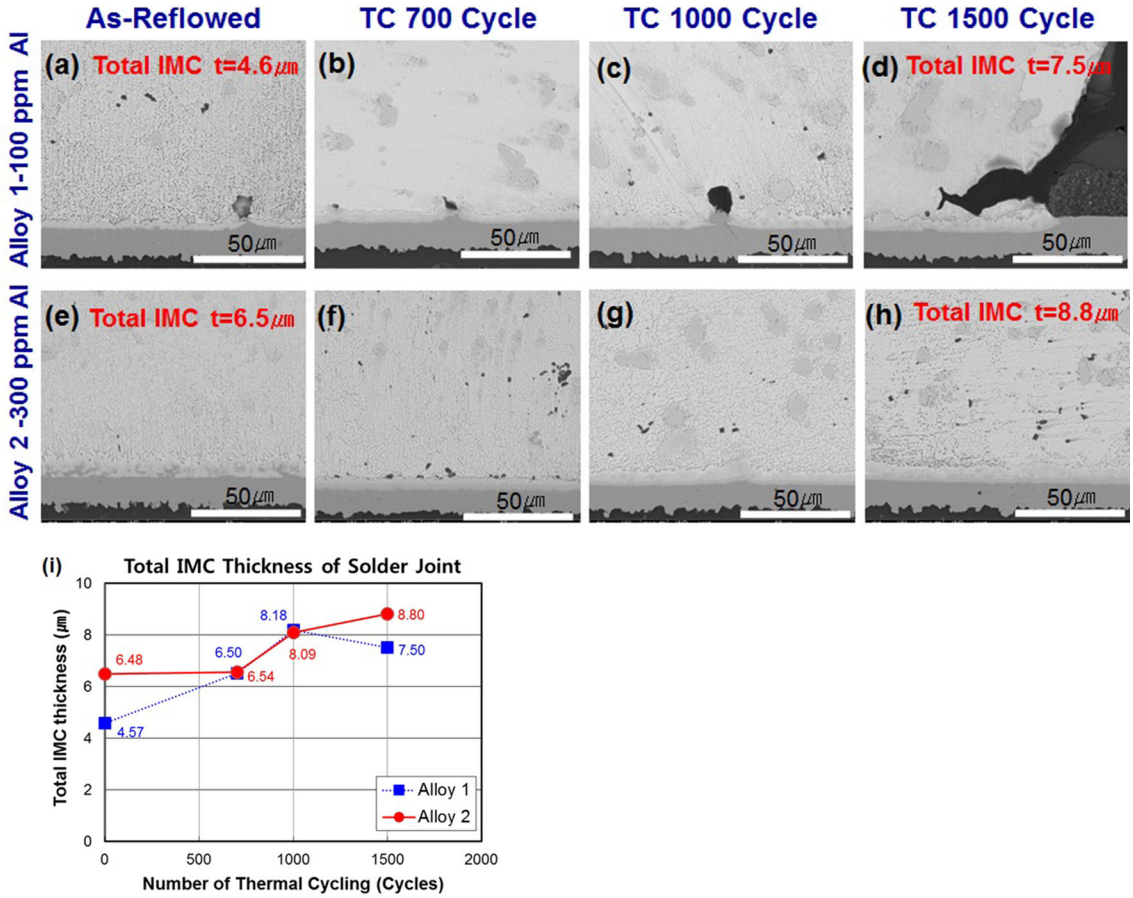

Fig. 11. SEM micrographs of total intermetallic compound (Cu_6Sn_5 + Cu_3Sn) layer thickness of solder joints with thermal cycling number: (a–d) alloy 1 and (e–h) alloy 2; (i) graph of IMC thickness.

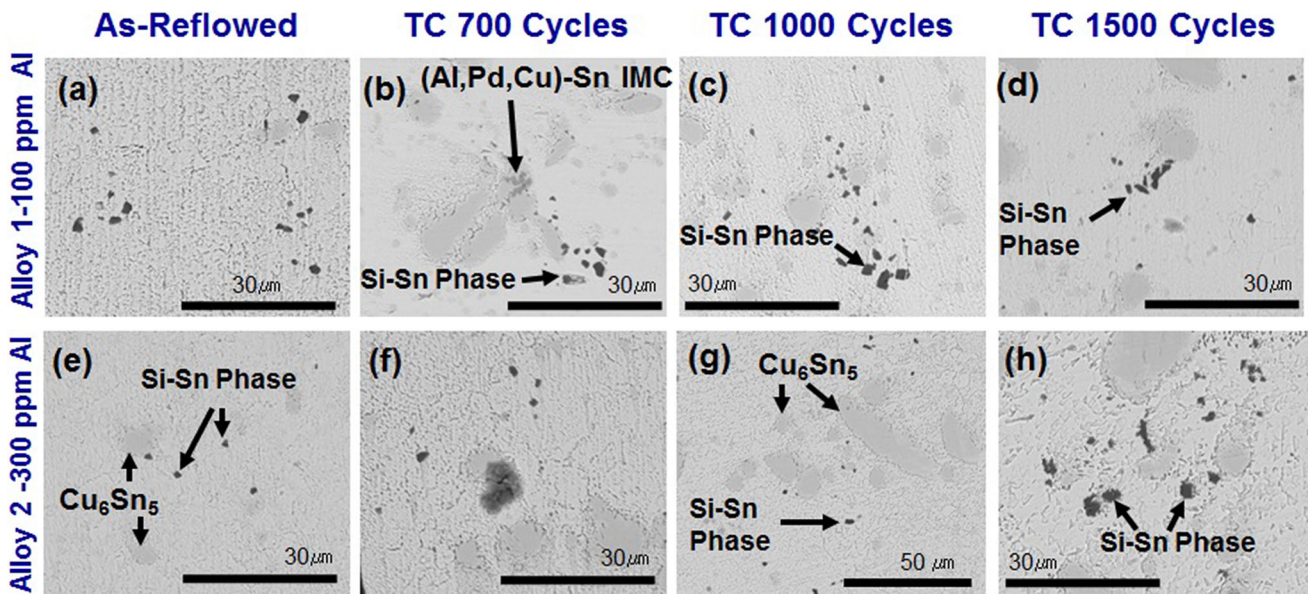

Fig. 12. Microstructure evolution of (a–d) 100 ppm and (e–h) 300 ppm Al alloying Sn-0.5Cu(Pd) solders with thermal cycling number.

increasing period of use.[16–18,22,23] However, the area ratio of the ductile and brittle fracture surfaces of the joints of alloys 1 and 2 was 30.8%–43.4%. Because of maintaining the ductility on the bulk solder and the interfaces, the brittle fracture area of the solder joint did not increase, compared to the

initial ductile and brittle fracture surface areas. The reason was supposed to the solder bulk evolution that causes the decrease of shear strength in Fig. 6. Therefore we could suppose that there was no degradation of shear strength after 700 cycles under thermal cycling conditions. An alternation of ductile and brittle fracture ratio with Al addition was not observed. Based on this result, in the case of 100 ppm–300 ppm Al addition into the Sn-0.5Cu solder alloy, the brittle fracture due to IMC growth at the solder joint can be suppressed. As shown in Figs. 10 and 11, maintaining the ductility of the solder with thermal cycling lead to a suppression of the shear strength degradation due to control of the IMC growth at the bulk solder and joints.

Intermetallic Compound Layer of Solder Ball Joints

Figures 10 and 11 show the cross-sectional micrographs of solder joints of alloys 1 and 2 with thermal cycling number. Although IMC growth was observed at the solder matrix, the irregular and needle-shaped IMC growth did not occur at the solder joints with the OSP finish rather than SAC305. Figure 11 shows the measurement results of total IMC (Cu_6Sn_5 + Cu_3Sn) layers of solder joints with thermal cycling number. The IMC thickness of the as-reflowed solder joints of alloys 1 and 2 was 4.57μm and 6.48 μm, which then grew to a maximum 7.5 μm and 8.8 μm after 1500 thermal cycles, respectively (Fig. 11i). Based on

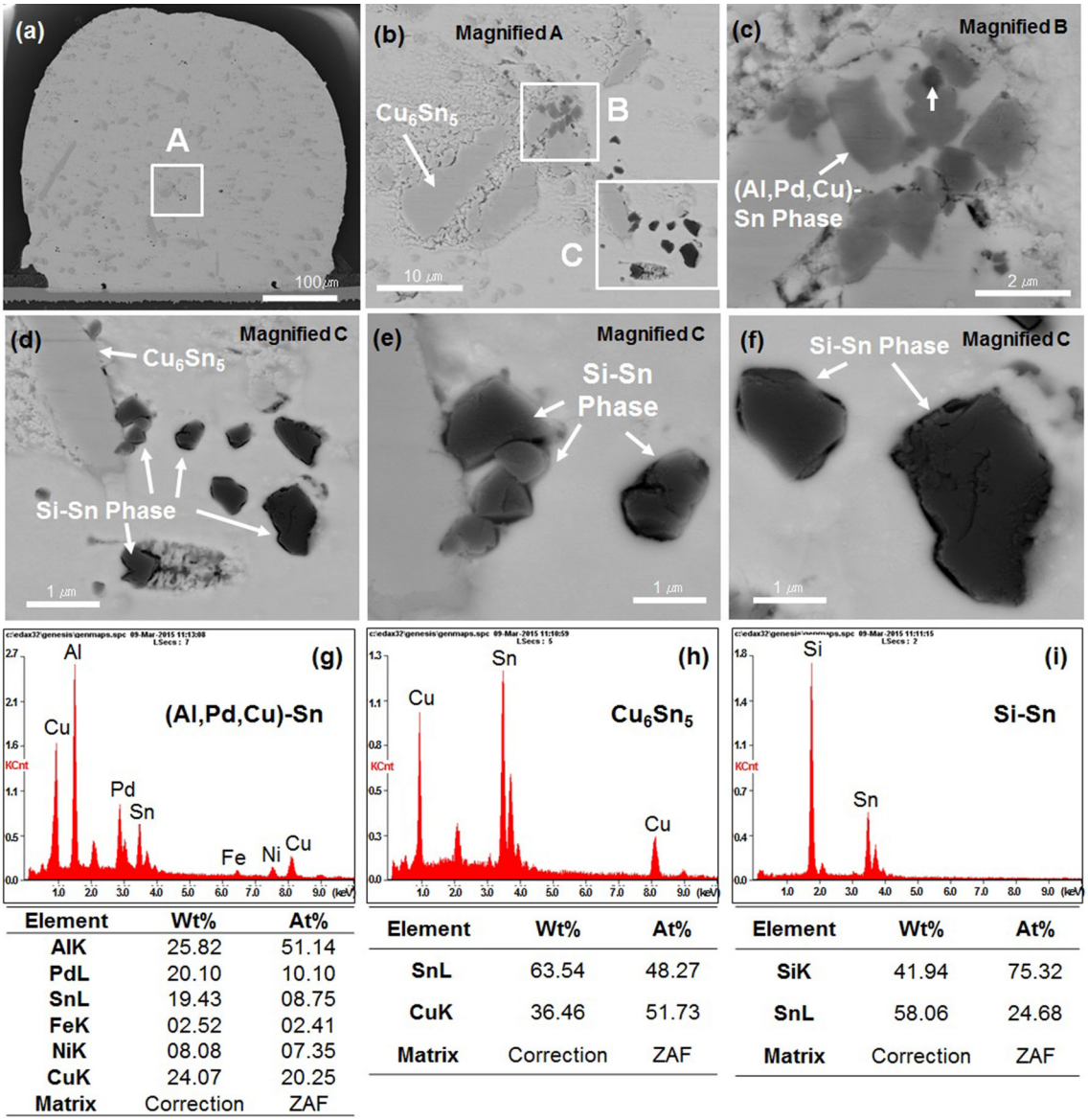

Element	Wt%	At%
AlK	25.82	51.14
PdL	20.10	10.10
SnL	19.43	08.75
FeK	02.52	02.41
NiK	08.08	07.35
CuK	24.07	20.25
Matrix	Correction	ZAF

Element	Wt%	At%
SnL	63.54	48.27
CuK	36.46	51.73
Matrix	Correction	ZAF

Element	Wt%	At%
SiK	41.94	75.32
SnL	58.06	24.68
Matrix	Correction	ZAF

Fig. 13. SEM micrographs of Sn-0.5Cu(Pd)-0.01Al(Si)-Ge solder alloy after 700 cycles of thermal cycling testing: (a) cross-sectional image of solder ball, (b–f) magnified views of A region in (a), and (g–i) EDS analysis results of (c–f).

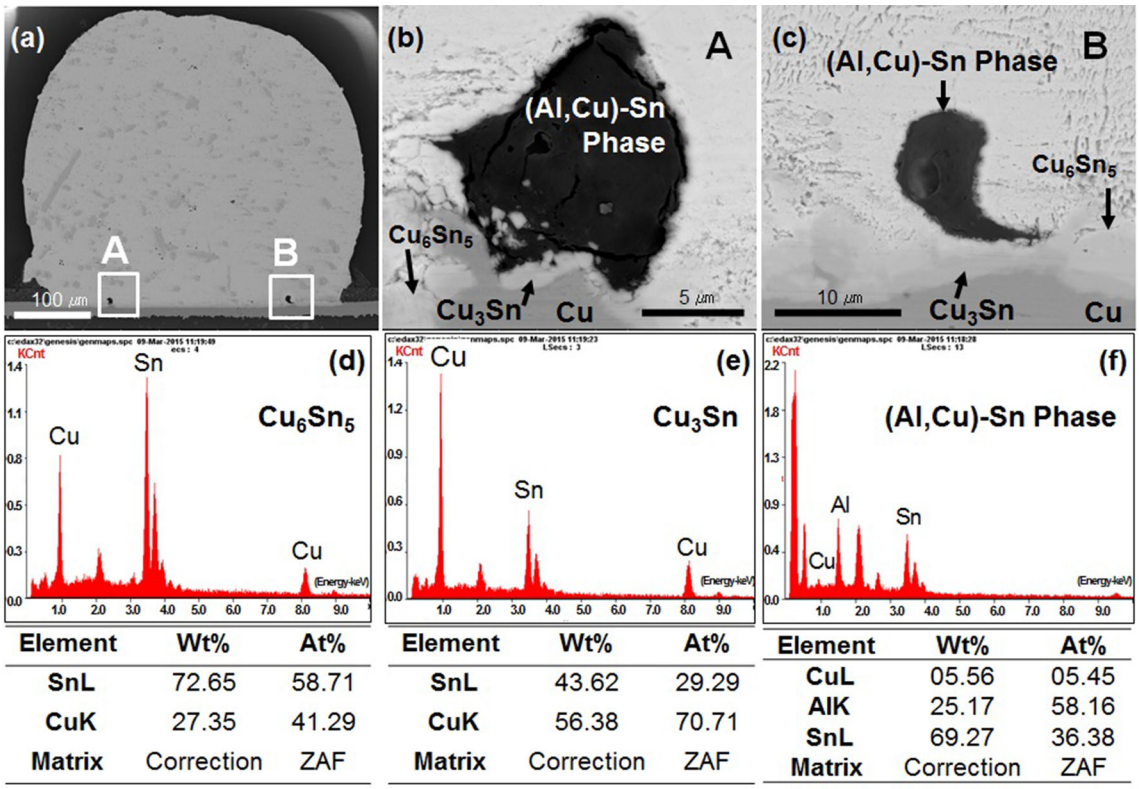

Fig. 14. SEM micrographs of Sn-0.5Cu(Pd)-0.01Al(Si)-Ge solder alloy after 700 cycles of thermal cycling testing: (a) cross-sectional image of solder ball, (b, c) magnified views of A and B regions in (a), and (d–f) EDS analysis results of Sn-rich phase and Cu–Sn IMCs in (b, c).

these results, we know that smaller Al-addition solder produces thinner and flat IMC layers compared with the the SAC305/Cu solder joint. In the case of Pd addition in the solder alloy, Pd can trap Cu and act as nucleation sites for the growth of $(Cu,Pd)_6Sn_5$[10,11] This heterogeneous nucleation in the solder might contribute to refining the grain structure and reducing Cu_6Sn_5 growth. In a recent publication about the effects of Pd addition from Lee et al.[11], the mechanical stability of solder joints with Pd added to Sn-Ag-Cu alloy showed more grain refinements, recrystallization, and, in particular, mechanical twin deformation during the shock testing, compared to SAC305. The additional influence of Pd on aging effects is that the IMC precipitates are finer and more stable.[11] The role of Al alloying to Sn-Ag-Cu is to avoid deleterious product phases, such as Ag_3Sn IMC. Ag_3Sn formation is suppressed for increased Al content (0.05–0.2 Al), and $Cu_{33}Al_{17}$ clustered particles improved thermal cycling reliability.[12,16,17] As seen in Fig. 11, the total IMC (Cu_6Sn_5 + Cu_3Sn) layer did not grow instead of the general Sn-Ag-Cu or Sn-Cu solder joints. Yu et al.[28] observed the spreadability and shear strength degradation with isothermal aging time of two Sn-0.5Cu + Al(Si) solder materials compared to commercial Sn-0.7Cu solder, and then the IMC shape and thickness was compared with the Sn-0.7Cu solder joints.[29–31] In this paper, IMC thickness was decreased with increasing the amounts of Al(Si). These results indicated Al(Si) alloying effects that could suppress IMC growth and improve the reliability of the solder joint. Consequently, we can suppose that IMC growth was suppressed by minor Pd and Al(Si) additions at the solder joint in alloys 1 and 2.

Microstructural Evolution of Solder Joints with Minor Al and Si Alloying Additions

The microstructural observation results of alloys 1 and 2 with thermal cycling are shown in Figs. 12 and 13. The Cu_6Sn_5 IMC is formed at the bulk of alloys 1 and 2 due to the major elements of the Sn-Cu solder. However, fine dispersive Si-Sn particles were observed at the matrix due to addition of Si. Also, upon increasing the thermal cycling number, the distribution of Sn-Si particles increased somewhat. We know that the Cu_6Sn_5 IMC did not grow after 700 and 1500 thermal cycles at the bulk solder. As mentioned for the Pd and Al addition effects, we know that minor alloying additions are effective in suppressing grain and IMC growth.[10–18]

To analyze the Cu–Sn IMC and Sn-Si observed in the previous figures, we conducted cross-sectional micrographs of the solder joint with thermal cycles. Figure 13 shows the SEM micrographs and EDS analysis results of alloy 1 after 700 thermal cycles.

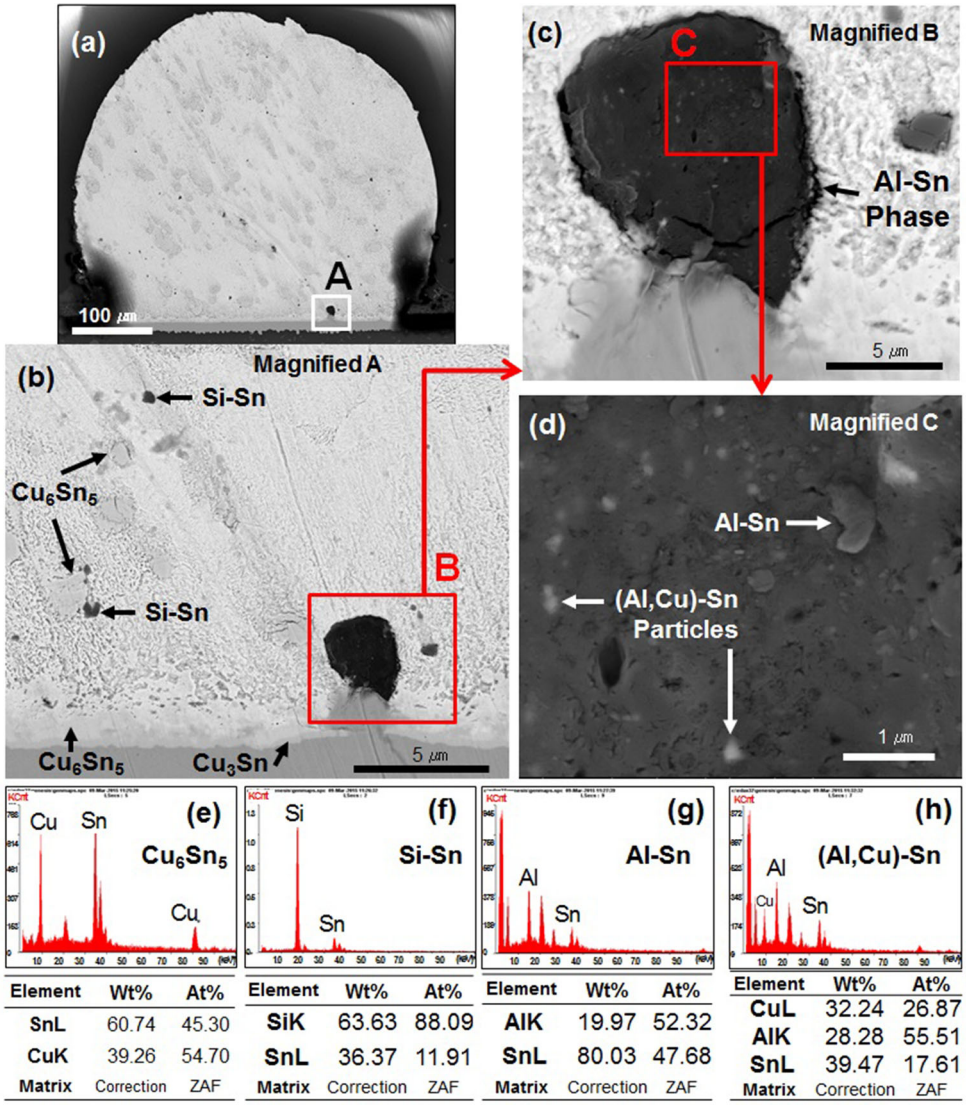

Fig. 15. SEM micrographs of Sn-0.5Cu(Pd)-0.01Al(Si)-Ge solder alloy after 1000 cycles of thermal cycling test: (a, b) cross-sectional image of solder ball, (c, d) magnified views of B and C regions in (b, c) respectively, and (e–h) EDS analysis results of Sn-rich phases and Cu–Sn IMCs.

Figure 13b is a magnified view of Fig. 13a. The different phases were observed at the B area (light gray color) and C area (deep gray color) around the Cu_6Sn_5 IMC in Fig. 13b. Based on the EDS results,the light gray particles were confirmed as the (Al, Pd,Cu)-Sn phase and the deep gray particles were the Si-Sn phase. These phases were cleated at the nucleation site of the Cu_6Sn_5 IMC during an initial solidification process after melting. Generally, it is well known that Cu_6Sn_5 is continuously created at the β–Sn site.[15–18] The solidification process of the Sn-0.5Cu + Al(Si) alloy was well explained by Koo's et al.[24] study about the order of the solidified phases during solidification. In the case of minor Al(Si) addition to the Sn-0.5Cu alloy, Cu–Al phases were formed at the solder matrix, and suppressed the formation of eutectic the β–Sn + Cu_6Sn_5 microstructure. Based on the thermodynamically calculated result of Koo et al., Cu–Al phases were solidified first, resulting in refined eutectic β–Sn + Cu_6Sn_5 networks, and then the primary β–Sn and eutectic β–Sn + Cu_6Sn_5 were continuously solidified.[24] Consequently, in the case of Al, Si and Pd additions to Sn-0.5Cu solder alloy, we can suppose that these elemental phases can also be created continuously first around the Cu_6Sn_5 IMC nucleation site.

As mentioned in Ref. 16, the addition of Al to Sn-Cu and SAC solders showed more than a 70% reduction in β–Sn undercooling because of the formation of the Cu–Al IMC, and, finally, the Cu–Al IMC reduced the occurrence of Ag_3Sn plates, a brittle phase in the SAC solder matrix.[12,16] The Cu–Al and Sn-Cu–Al IMC phases in molten solder during alloy fabrication have the potential to be a means of strengthening and extending the lifetime of solder joints in microelectronics applications (Cu–

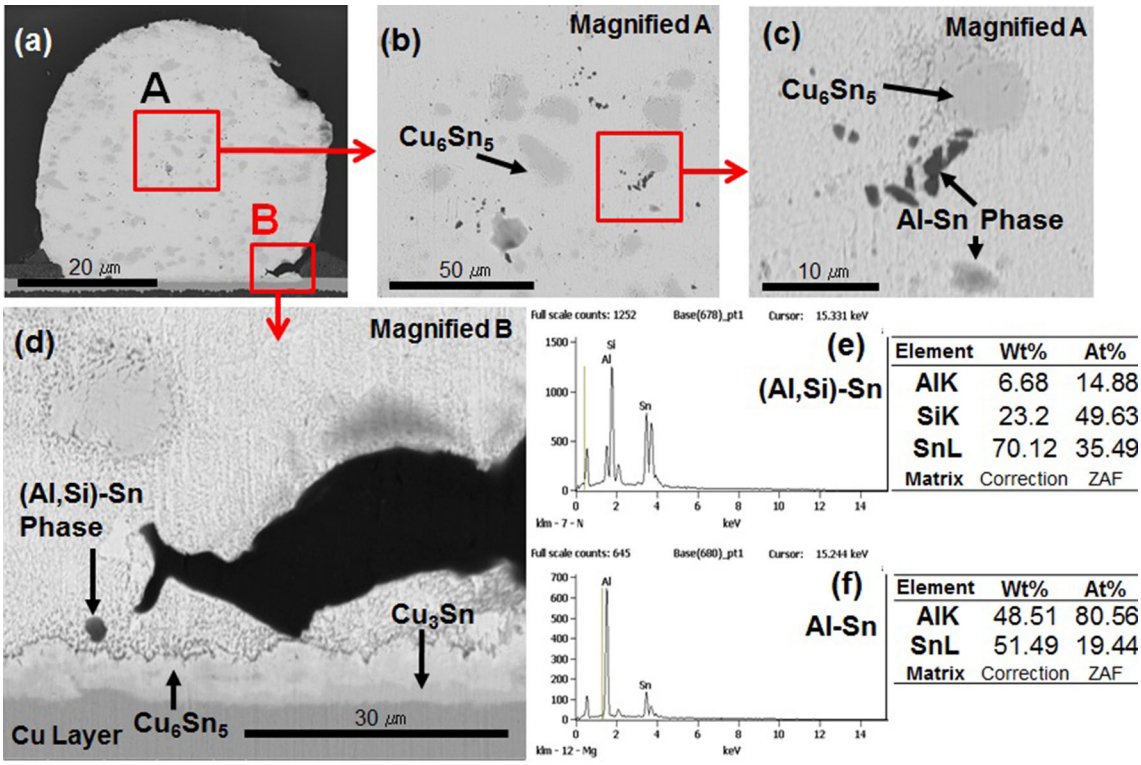

Fig. 16. SEM micrographs of Sn-0.5Cu(Pd)-0.01Al(Si)-Ge solder alloy after 1500 cycles of thermal cycling test: (a) cross-sectional image of solder ball, (b, c) magnified views of A and B regions in (a), and (d–f) EDS analysis results of Sn-rich phase and Cu–Sn IMCs.

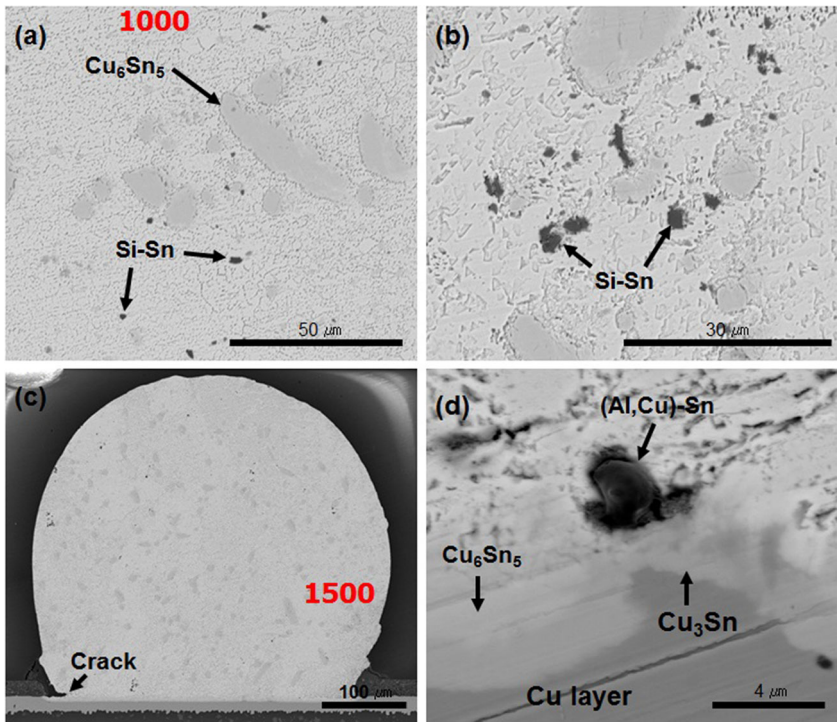

Fig. 17. SEM images of 300 ppm Al alloy addition after (a) 1000 cycles and (b–d) 1500 cycles of thermal cycling.

Al IMC, $Cu_{33}Al_{17}$).[12–16] According to the previous study by Reeve,[16] in the case of 0.05–0.10 wt.% Al addition to SAC alloy, the formation of Ag_3Sn particles was eliminated. Al addition to Sn-Cu alloys revealed refinement of the Cu_6Sn_5 IMC for a range of Al addition from 250 ppm to 2000 ppm.

The effect of Al on the refinement of IMCs, specifically Cu_6Sn_5 in Sn-Cu alloys Ag_3Sn, has been demonstrated in several studies.[12–18]

Figure 14 shows the SEM and EDS analysis results of alloy 1 after 700 thermal cycles. The (Al,Cu)-Sn phase (black color, Fig. 14c) was observed at the solder joint. The (Al,Cu)-Sn phase mainly existed at the interface between Cu_6Sn_5, Cu_3Sn and the solder matrix. In the case of the Si-Sn phase observed at the bulk, we can understand a similar mechanism with Cu_6Sn_5 nucleation process at the same site. Therefore, we can suppose that the (Al,Cu)-Sn phase formed at the interface is created with a Sn combined phase and Cu_6Sn_5 during the Cu_6Sn_5 nucleation process. However, as the Sn-Si phase did not exist at the interface, we can suppose that the Sn-Si phase was formed at the solder matrix by a different process. Such phase formation processes need to be analyzed in more detail.

The analysis of the (Al,Cu)-Sn phase at the solder joint of alloy 1 after 1000 cycles is shown in Fig. 15. Similar to Fig. 14, the Al–Si and (Al,Cu)-Sn phases were observed at the solder joint, withSi-Sn particles dispersed around Cu_6Sn_5 in the solder matrix. Figure 15d is the magnified view of the Al–Si phase in Fig. 15c. Fine white particles were dispersed in the Al–Si phase (dark gray color), which was found in the (Al,Cu)-Sn phase (Fig. 15g). According to these analysis results, when the IMC formed at the solder joint, the Al–Si phase was created at the same time, and then the (Al,Cu)-Sn phases were formed and dispersed in the Al-Sn phase due to the reaction of the Al-Sn phase and Cu. Because these particles act to suppress crack generation and propagation at the interfaces, the reliability of the Sn-0.5Cu(Pd)-0.01Al(Si)-Ge solder joint was superior to the Sn-Ag-Cu solder.

Figure 16 shows the cross sectional micrographs of alloy 1 after 1500 thermal cycles. Figure 16b and c show the enlarged view of the solder bulk and Al-Sn phase dispersed around the Cu_6Sn_5 IMC. Also, the first corner crack was observed at the solder joint (Fig. 16d), with the shape of a traditional fatigue crack. The (Al,Cu)-Sn phases (dark gray color) existed at the crack tip and it contained Al and Si. According to the previous study by Anderson et al.[16], when Al was included at a minimum of 0.5 wt.%, we could expect the solder joint reliability of the SAC305 solder to improve. However, in this study, we found that the effect with 0.01 wt.% Al and Si addition was to suppress the bonding strength degradation and microstructure growth. Therefore, if minor amounts of Pd, Al and Si are added to the Sn-0.5Cu solder, we can expect a relaxation in the bonding strength degradation of the solder joint.

Figure 17 shows the cross-sectional micrographs of alloy 2 after 1000 and 1500 thermal cycles. Compared to Fig. 17a and b, the Cu_6Sn_5 IMC in the solder matrix did not grow with thermal cycling number, and the Si-Sn phase dispersed around the Cu_6Sn_5 IMC. In the case of minor Al and Si addition similar to the nucleation of Cu–Al phases in the Sn-0.5Cu matrix, the Si-Sn phase was observed around the Cu_6Sn_5 IMC and Cu–Al phases. Even though it needs more quantitative analysis, we can suppose that the addition of Si contributed to the suppression of IMC growth because the Si-Sn phase consumed the Sn supply needed for Cu_6Sn_5 IMC growth, similar to the Al addition effect. The corner crack and (Al,Cu)-Sn phase were observed at the solder joint (Fig. 17c). The (Al,Cu)-Sn phase (Fig. 17d) existed between Cu_6Sn_5 and Cu_3Sn. When observed in more detail, Cu_3Sn existed under the (Al,Cu)-Sn phase, but not the Cu_6Sn_5 IMC layer. Finally, similar to the solder matrix, Al added to Sn-0.5Cu formed the (Al,Cu)-Sn phase, and the solder joint reliability was improved by suppressing Cu_6Sn_5 and Cu_3Sn IMCs at the solder joint.

CONCLUSIONS

To improve solder joint reliability for automotive engine compartment electronics, we proposed mid-temperature Sn-0.5Cu-based solder alloys (Sn-0.5Cu(Pd)-0.01Al(Si)-0.006Ge and Sn-0.5Cu(Pd)-0.03Al(Si)-0.007Ge) which contained minor additions of Pd, Al, Si and Ge. To verify their solder joint reliability, we used thermal cycling from 40°C to 125°C for 1500 cycles. Although shear strength degradation was similar to the Sn-3.0Ag-0.5Cu solder for 700 thermal cycles, the degradation rate from 700 to 1500 cycles decreased remarkably. This reason for this was the suppression of Cu_6Sn_5 and Cu_3Sn IMC growth at the solder joint due to the Pd addition, and also the irregular-shaped IMC changed to a flat shape. Si-Sn, Al-Sn and (Al,Cu)-Sn phases were observed in the solder matrix and around the Cu_6Sn_5 IMC. These phases suppressed IMC growth at the interfaces and matrix due to the dispersion around the IMC. In particular, the shear strength degradation of the 0.01 wt.% Al addition solder showed a smaller degradation than that of the 0.03 wt.% Al alloying. According to these results, with a very small amount (100 ppm–300 ppm) of Al, Si, Pd and Ge alloying elements, we confirmed the possibility of using a Sn-0.5Cu–0.01Al(Si)-Ge solder in automotive engine compartment electronics.

REFERENCES

1. European Union Council, Directive 2000/53/EC of the European Parliament and of the Council of 18 September 2000 on end-of life vehicle (ELV, 2003). http://ec.europa.eu/environment/waste/elv/index.htm. Accessed 29 Feb 2016.
2. I.E. Anderson and R.L. Terpstra, U.S. Patent No. 6,231,691 (2001).
3. W.S. Hong and C.M. Oh, *J. KWJS* 31, 22 (2013).
4. Y.-H. Ko, S.H. Yoo, and C.-W. Lee, *J. Microelectron. Packag. Soc.* 17, 35 (2010).
5. C.M. Oh, N.C. Park, and W.S. Hong, *J. Kor. Inst. Met. Mater.* 46, 80 (2008).
6. R.W. Johnson, J.L. Evans, P. Jacobsen, J.R. Thompson, and M. Christopher, *IEEE Trans. Electron. Packag. Manuf.* 27, 164 (2004).

7. S.-S. Ha, S.-B. Jung, J.-W. Kim, J.-H. Chae, W.-C. Moon, T.-H. Hong, C.-S. Yoo, J.-H. Moon, S.-B. Jung, and J. Kor, *Weld. Join. Soc.* 24, 21 (2006).
8. W.S. Hong, W.S. Kim, B.S. Song, and K.-B. Kim, *Kor. J. Mater. Res.* 17, 152 (2007).
9. W.S. Hong and A.Y. Kim, *Mater. Trans. JIM* 56, 1002 (2015).
10. I.-T. Wang, J.-G. Duh, C.-Y. Cheng, and J. Wang, *Mater. Sci. Eng. B* 177, 278 (2012).
11. T.-K. Lee, B. Zhou, T. Biler, C.-F. Tseng, and J.-G. Duh, *J. Electron. Mater.* 42, 215 (2013).
12. A.J. Boesenberg, I.E. Anderson, and J.L. Harringa, *J. Electron. Mater.* 41, 1868 (2012).
13. C.M. Miller, I.E. Anderson, and J.F. Smith, *J. Electron. Mater.* 23, 595 (1994).
14. K.W. Moon, W.J. Boettinger, U.R. Kattner, F.S. Biancaniello, and C.A. Handwerker, *J. Electron. Mater.* 29, 1122 (2000).
15. I.E. Anderson, J.K. Walleser, J.L. Harringa, F. Laabs, and A. Kracher, *J. Electron. Mater.* 38, 2770 (2009).
16. K.N. Reeve, I.E. Anderson, and C.A. Handwerker, *J. Electron. Mater.* 44, 842 (2015).
17. S.D. Mcdonald, K. Nogita, J. Read, T. Ventura, and T. Nishimura, *J. Electron. Mater.* 42, 256 (2013).
18. K. Sweatman, T. Nishimura, S.D. McDonald, M. Whitewick, and K. Nogita, *SMT Mag.* 29, 30 (2014).
19. S.J. Hong, K.S. Kim, C.W. Lee, J. H. Bang, Y.H. Ko, H.M. Lee, J.W. Chang, J, H. Koo, J.T. Moon, Y.W. Lee, W.S. Hong, H.J. Kim, and J.H. Lee, U.S. Patent No. 9,156,111 B2 (2015).
20. A.Y. Kim and W.S. Hong, *J. Weld Join* 32, 288 (2014).
21. A.Y. Kim, C.M. Oh, and W.S. Hong, *J. Weld Join* 33, 239 (2015).
22. L. Ladani and J. Razmi, *J. Electron. Mater.* 40, 573 (2012).
23. W. Zhou, L. Liu, and P. Wu, *Intermetallics* 18, 922 (2010).
24. J.H. Koo, C.S. Lee, S.J. Hong, K.-S. Kim, and H.M. Lee, *J. Alloys Comp.* 650, 106 (2015).
25. M.F.M. Sabri, D.A. Shnawah, I.A. Badruddin, and S.B.M. Said, *J. Alloys Compd.* 582, 437 (2014).
26. M.E. Alam and M. Gupta, *Electron. Mater. Lett.* 10, 515 (2014).
27. J.F. Li, P.A. Agyakwa, and C.M. Johnson, *J. Alloys Compd.* 545, 70 (2012).
28. D.Y. Yu, Y.-H. Ko, J.H. Bang, and C.W. Lee, *J. Weld. Join.* 33, 19 (2015).
29. J.H. Bang, D.Y. Yu, Y.-H. Ko, J.-W. Yoon, and C.W. Lee, *J. Weld. Join.* 34, 26 (2016).
30. J.W. Teo, *IEEE Trans. Electron. Packag. Manuf.* 30, 279 (2007).
31. J.H.L. Pang, T.H. Low, B.S. Xiong, X. Luhua, and C.C. Neo, *Thin Solid Films* 462, 370 (2004).